Current Research in Physiology 5 (2022) 404–413

Contents lists available at ScienceDirect

Current Research in Physiology

journal homepage: www.sciencedirect.com/journal/current-research-in-physiology

Effect of an autism-associated *KCNMB2* variant, G124R, on BK channel properties

Hans J. Moldenhauer [a], Ria L. Dinsdale [a], Sara Alvarez [b], Alberto Fernández-Jaén [c], Andrea L. Meredith [a,*]

[a] Dept. of Physiology, University of Maryland School of Medicine, Baltimore, MD, USA
[b] NimGenetics, Madrid, Spain
[c] Dept. of Pediatric Neurology, Hospital Universitario Quirónsalud, School of Medicine, Universidad Europea de, Madrid, Spain

ARTICLE INFO

Keywords:
BK channel
KCa1.1
Calcium-activated potassium channel
KCNMA1
Potassium channel
MaxiK
Slo
Slowpoke
Channelopathy
Autism
Intellectual disability
KCNMB2
beta2
Inactivation

ABSTRACT

BK K^+ channels are critical regulators of neuron and muscle excitability, comprised of a tetramer of pore-forming αsubunits from the *KCNMA1* gene and cell- and tissue-selective β subunits (*KCNMB1-4*). Mutations in *KCNMA1* are associated with neurological disorders, including autism. However, little is known about the role of neuronal BK channel β subunits in human neuropathology. The β2 subunit is expressed in central neurons and imparts inactivation to BK channels, as well as altering activation and deactivation gating. In this study, we report the functional effect of G124R, a novel *KCNMB2* mutation obtained from whole-exome sequencing of a patient diagnosed with autism spectrum disorder. Residue G124, located in the extracellular loop between TM1 and TM2, is conserved across species, and the G124R missense mutation is predicted deleterious with computational tools. To investigate the pathogenicity potential, BK channels were co-expressed with $\beta2^{WT}$ and $\beta2^{G124R}$ subunits in HEK293T cells. BK/β2 currents were assessed from inside-out patches under physiological K^+ conditions (140/6 mM K^+ and 10 μM Ca^{2+}) during activation and inactivation (voltage-dependence and kinetics). Using β2 subunits lacking inactivation (β2IR) revealed that currents from BK/$\beta2IR^{G124R}$ channels activated 2-fold faster and deactivated 2-fold slower compared with currents from BK/$\beta2IR^{WT}$ channels, with no change in the voltage-dependence of activation ($V_{1/2}$). Despite the changes in the BK channel opening and closing, BK/$\beta2^{G124R}$ inactivation rates (τ_{inact} and $\tau_{recovery}$), and the $V_{1/2}$ of inactivation, were unaltered compared with BK/$\beta2^{WT}$ channels under standard steady-state voltage protocols. Action potential-evoked current was also unchanged. Thus, the mutant phenotype suggests the $\beta2^{G124R}$ TM1-TM2 extracellular loop could regulate BK channel activation and deactivation kinetics. However, additional evidence is needed to validate pathogenicity for this patient-associated variant in *KCNMB*2.

1. Introduction

Autism spectrum disorder (ASD) is a neurodevelopmental condition linked to inherited and *de novo* genetic changes that includes repetitive behavior, impaired social interaction, and impaired verbal/non-verbal communication (El-Fishawy and State, 2010; Wisniowiecka-Kowalnik and Nowakowska, 2019). To date, more than 102 gene mutations have been linked to ASD (Satterstrom et al., 2020) including ion channels and their regulatory subunits (Schmunk and Gargus, 2013). Among the K^+ channels associated with ASD are *KCNMA1* and *KCNMB4*, genes encoding the large conductance 'BK' calcium- and voltage-activated K^+ channel and its modulatory subunit β4, respectively. Both *KCNMA1* mutations and single nucleotide polymorphisms (SNPs) have been linked to ASD or related phenotypes, such as intellectual disability and developmental delay (Bailey et al., 2019; Miller et al., 2021; Laumonnier et al., 2006; Staisch et al., 2016; Song et al., 2018; Plante et al., 2019; Wu et al., 2020; Yesil et al., 2018; Perche et al., 2022). BK channel activity is altered in several Fragile X and Angelman human patient and animal ASD models, associated with increased neuronal excitability that can be reversed via BK channel modulation (Contractor et al., 2015; Deng and Klyachko, 2016; Deng et al., 2013; Sun et al., 2019; Valerie Lemaire-Mayo et al., 2020; Hurley et al., 2021). One such modulation occurs through the β4 subunit, and both BKα and BK/β4 channels directly interact with Fragile X mental retardation protein (FMRP) to

* Corresponding author. Dept. of Physiology University of Maryland School of Medicine, 655 W. Baltimore St. Baltimore, MD, 21201, USA.
E-mail address: ameredith@som.umaryland.edu (A.L. Meredith).

https://doi.org/10.1016/j.crphys.2022.09.001
Received 11 June 2022; Received in revised form 26 August 2022; Accepted 20 September 2022
Available online 25 September 2022

alter activation and deactivation gating kinetics and channel open probability (Deng et al., 2013; Deng and Klyachko, 2016; Kshatri et al., 2020). Thus, changes in BK channel activity via a *KCNMA1* mutation, or through an accessory β subunit (β4), are associated with ASD-like features. However, little is known about β2, a neuron and endocrine-expressed β subunit modulating BK channel activity that is widely expressed in brain (Brenner et al., 2000b).

Both β2 and β4 subunits provide unique phenotypes to the BK channel that alter BK channel activity (Gonzalez-Perez and Lingle, 2019). BK channel expression overlaps with both β2 and β4 in central neurons (Latorre et al., 2017; Tseng-Crank et al., 1996), with β4 typically more highly expressed compared with β2 (Brenner et al., 2000b). While both subunits slow gating kinetics, β2 predominantly confers an inactivation via pore occlusion from the intracellular N-terminus, reducing BK channel activity (Brenner et al., 2000b; Jaffe et al., 2011). Additionally, β2 and β4 affect the calcium sensitivity of BK channels, but in different ranges (Brenner et al., 2000a). Thus, both accessory subunits are able to reduce the BK channel activity through different mechanisms, leading to multiple possibilities for alteration of neuronal excitability. While only β4 function is implicated in ASD-related learning disability at present, genome-wide association studies have recently identified *KCNMB2* SNP associations in autism case trios and other neuropathological states (Beecham et al., 2014; Kimbrel et al., 2018; Xia et al., 2020). β2 expression has been detected in several areas of the brain implicated in ASD (Brenner et al., 2000b; Nordahl et al., 2012; Schumann et al., 2004; Stoodley, 2014).

In this study, we characterize a new patient-derived *KCNMB2* variant (G124R) from a child diagnosed with ASD as a primary clinical presentation. Electrophysiological investigation of $\beta2^{G124R}$ was performed on a brain-expressed BK channel isoform, using voltage protocols designed to assess the effect of G124R on steady-state BK/β2 channel activation and inactivation properties and action potential-evoked BK current levels. Our results show that G124R alters the BK/β2 activation and deactivation kinetics, without affecting the inactivation phenotype, defining a functional consequence for the mutation on BK current properties.

2. Methods

2.1. Genetic and bioinformatic analysis

Exome sequencing was performed using genomic DNA isolated from whole blood from proband and parents (MagnaPure, Roche). Libraries were prepared using the Ion AmpliSeq™ Exome Kit (Life Technologies) and quantified by qPCR. The enriched libraries were prepared using Ion Chef™ and sequenced on PI™ Chip in the Ion Proton™ System (Life Technologies) to provide >90% of amplicons covered by at least 20X. Signal processing, base calling, alignment and variant calling were performed on a Proton™ Torrent Server using the Torrent Suite™ Software. Variants were annotated using Ion Reporter™ Software, and pedigree analysis was performed using the Genetic Disease Screen (GDS) trio workflow. Variant filtering and prioritization were performed using an in-house software program and a local database. Candidate variants were visualized using IGV (Integrative Genomics Viewer) and confirmed by Sanger sequencing. Candidate variants were evaluated at both the gene and variant levels, based on patient phenotype and the inheritance pattern and classified following the American College of Medical Genetics and Genomics (ACMG) guidelines. A molecular clinical geneticists board evaluated each variant for classification as pathogenic, likely pathogenic, or variant of uncertain significance (VUS) for reporting. The study was carried out in accordance with the Declaration of Helsinki of the World Medical Association and approved by the Local Ethics Committees (Madrid, Spain; Ref. 30062019). Informed consent was obtained from parents, after full explanation of the procedures.

The β2 homology model Q9CZM9 was obtained from the Swiss-model protein repository (https://swissmodel.expasy.org/repository/) and is made using the β4 cryoEM structure 6V35 (Tao and MacKinnon, 2019) as a template. The primary sequence alignment was performed in Uniprot (https://www.uniprot.org/align/) between the β2 sequences: human Q9Y691, rat Q811Q0, mouse Q9CZM9, pig F1SGC9 and cow Q1RW7. Pathogenicity predictor tools REVEL (Rare Exome Variant Ensemble Learner), CADD (Combined Annotation Dependent Depletion), MetaLR (Meta Logistic Regression) and Mutpred were obtained online at the Ensembl website (https://www.ensembl.org/Tools/VEP) (Dong et al., 2015; Ioannidis et al., 2016; Pejaver et al., 2020; Rentzsch et al., 2019).

2.2. Patch-clamp electrophysiology

The human *KCNMA1* (BKα subunit) (MG279689) and human *KCNMB2* ($\beta2^{WT}$) cDNA sequences were expressed from the pcDNA3.1+ mammalian expression vector (Brenner et al., 2000a; Whitt et al., 2016). Inactivation was removed by deleting the Phe-Ile-Tyr residues (ΔFIW), resulting in the construct called β2IR (IR: Inactivation Removed) (Wallner et al., 1999; Wang et al., 2002; Whitt et al., 2016). Gly124Arg (rs201338193; GGG to AGG) was introduced into the $\beta2^{WT}$ and β2IR backgrounds and verified by sequencing. The BK channel contained a N-terminal extracellular Myc tag and EYFP in RCK2, used to identify transfected cells. The Myc and EYFP inserts do not affect the BK channel properties (Plante et al., 2019). The BK channel and β2 plasmids were transfected into HEK293T cells as previously described (Moldenhauer et al., 2020; Whitt et al., 2016), in a ratio 1:2 (0.9 μg BKα and 1.8 μg β2, respectively). Electrophysiological recordings were performed 24 h post-transfection.

Macroscopic BK currents were obtained in the inside-out patch-clamp configuration at room temperature (RT: 22–24 °C) (Moldenhauer et al., 2020). Recordings were performed in physiological K^+ conditions, with the pipette solution (in mM): 134 NaCl, 6 KCl, 1 $MgCl_2$, 10 glucose, and 10 HEPES (pH7.4 with NaOH), and the internal (bath) solution (in mM): 110 $KMeSO_3$, 10 NaCl, 30 KCl, 10 HEPES, 1 $MgCl_2$, 5 HEDTA and adding Ca2+ to have 10 μM $CaCl_2$ (pH 7.2 with KOH). E_K was −75 mV. The free Ca^{2+} concentration was calculated with WebMaxC (http://web.stanford.edu/~cpatton/webmaxcS.htm). Voltage protocols were applied using a MultiClamp700B amplifier and CLAMPEX v10.3 (Molecular Devices, Sunnyvale, CA). Current traces were acquired at 50 kHz and filtered online at 10 kHz (pClamp 10.6, Molecular Devices). Two protocols were used to assess activation and deactivation, respectively, from BK + $\beta2IR^{WT}$ or $\beta2IR^{G124R}$. The activation protocol stepped from a V_{hold} of −120 mV, then from −100 to +100 mV (Δ+10 mV increments) for 30 ms, and stepping back to −150 mV for 15 ms to generate tail currents. Normalized conductance (G/G_{max}) was calculated from the current level 150–200 μs after the peak of the tail current, divided by the highest conductance value calculated for each patch. Conductance-voltage (G/G_{max}-V) curves were fitted with a Boltzmann function, constrained between 0 and 1, to obtain the half-maximal voltage of activation ($V_{1/2}$) (Prism v9.0.0, GraphPad Software, San Diego, CA) as described in Moldenhauer et al. (2020). Only patches with maximal $V_{1/2}$ shifts (>2 S.D. from the first quartile average) were included. Activation time constants (τ_{act}) were obtained single exponential fits of the current rise to the steady-state (SS) phase. The second voltage protocol was used to obtain τ_{deact}: From −150 mV (V_{hold}), the protocol steps to +200 mV for 20 ms for activation, followed by steps from −200 mV to −50 mV (Δ+10 mV increments) for 15 ms. τ_{deact} was obtained from single exponential fits of the peak of the tail current to the SS.

Inactivation was assessed from BK + $\beta2^{WT}$ or $\beta2^{G124R}$ co-expression. Inactivation kinetics (τ_{inact}) and the half maximal voltage of the steady-state inactivation ($V_{1/2\_inact}$) were determined from square voltage steps from −120 mV (V_{hold}), stepping to −200 to +200 mV (Δ+20 mV increments) for 150 ms, followed by +160 mV post-pulse, and back to −120 mV for 15 ms. The inter-sweep time was 2–3 s at the V_{hold}. τ_{inact} was obtained from a single exponential fit of the macroscopic current

decay. $V_{1/2\_inact}$ was obtained from a Boltzmann fit to the normalized maximum current obtained from the post-pulse, I_{+160}/I_{max}. A two-pulse protocol was used to determine the kinetics of recovery from inactivation, $\tau_{Recovery}$. From −120 mV (V_{hold}), the voltage was stepped to +160 mV for 150 ms, stepping back to −150 mV, followed by a +160 mV post-pulse 10 ms duration at increments of 2 ms. The post-pulse maximal current was normalized by the maximum current from the activation step (I_{recov}) and was plotted against time to obtain a single exponential fit for $\tau_{Recovery}$. For action potential (AP)-activated currents, patches were first evaluated to determine the stoichiometry of the BK/β2 channel complex using an initial step to +160 mV for 150 ms. In patches where the τ_{inact} was 20 ± 5 ms (Wang et al., 2002), corresponding to full stoichiometry with 4 β2 subunits, a representative hypothalamic neuronal AP waveform was applied as the voltage command (Shelley et al., 2013). The area under the curve (AUC) was calculated from 4 ms before and after the maximum peak current evoked by the AP command and normalized to the maximum peak current evoked by the initial square voltage step to +160 mV. In all protocols, leak current was subtracted with a P/5 protocol using a V_{hold} sub sweep between −120 and −150 mV.

Statistical analysis was performed in Prism v9.0.0. BK channel ± BK/β2IR (WT and G124R) $V_{1/2}$, activation, and deactivation values were compared using a one-way ANOVA with Bonferroni post-hoc test. For BK/β2 (WT and G124R), $V_{1/2\_inact}$, inactivation kinetics, and AUC (AP-evoked current) comparisons were made with an unpaired t-tests. All data in figures are presented as mean ± SEM (lines and whiskers), with the individual data points for each patch.

3. Results

3.1. Patient case description

The proband is a 12-year-old male diagnosed with autism spectrum disorder (ASD) and mild intellectual disability, with predominant impairment of language and attention abilities. Partum occurred via uncomplicated vaginal delivery after 40-weeks of pregnancy. Birth weight was 3600 gr (60th percentile), length 53 cm (90th percentile), occipitofrontal diameter (OFD) 36.5 cm (90th percentile). Family history was not relevant; his parents are healthy. His first single syllable utterances and first verbal words were said at 1.5 and 6 years of age, respectively. He walked at 1.5 years old.

At 5 years, the patient showed verbal and nonverbal communication deficits, lack of joint attention, avoidance of mutual eye contact, stereopathy, and idiosyncratic language associated with hyperkinetic behavior. He received risperidone to improve these behaviors. The patient was placed on atomoxetine at age 8 for attention deficits. This therapy, at doses of 1.2 mg/kg/d, was associated with clear improvement in attention impulsiveness and social adaptation at school. He thus continues 1.2 mg/kg/d of atomoxetine daily and was enrolled in a conventional school system with supports. He maintained good behavior and average school performance.

At 11 years old, the clinical examination disclosed a weight of 35 kg (45th percentile), a height of 145 cm (70th percentile), and an OFD of 54 cm (60th percentile), without dysmorphic features. Routine laboratory screening including thyroid function and neurometabolic tests were within the normal range. Sleep video-EEG test and auditory evoked potentials displayed normal results. Brain 3T MRI did not reveal any significant structural malformations. Conventional genetic studies (karyotype and array comparative genomic hybridization analysis) revealed no abnormalities. Further information was obtained using the Autism Diagnostic Interview-Revised (ADI-R) and the Autism Diagnostic Observation Scale (ADOS) (Connolly et al., 2013; Fitzgerald, 2010). He met the criteria for autism spectrum disorder on both instruments.

Whole-exome sequencing (WES) revealed a heterozygous missense mutation in exon 4 of the *KCNMB2* gene on human chromosome 3q26.3 (Gene ID: 10242): NM_181361.3; c.370G > A; p.Gly124Arg (rs201338193). The allele frequency of this variant in the general population is 0.0092% (gnoMAD v2.1.1), with a higher frequency in Asian population (0.055%). No homozygous variant carriers have been described. In the WES trio analysis, the G124R variant was not present in either parent. No other missense variants with a CADD score over 15 (Rentzsch et al., 2019), nor LOF variants with a clear phenotypic association, were identified in the patient DNA.

3.2. In silico structural analysis of the G124R mutation in the β2 subunit

Genomic computational analyses predicted G124R as a pathogenic variant, with a CADD score of 29.6. This prediction was further supported by tools incorporating additional structural and functional properties, including Mutpred (score of 0.917), REVEL (0.543), and CADD PHRED (31), but not MetaLR (0.111) (Dong et al., 2015; Ioannidis et al., 2016; Pejaver et al., 2020; Rentzsch et al., 2019) (Fig. 1C). A Mutpred score of 0.8 yields a 5% probability of a false positive, thereby a score of 0.917 had a 0.5% probability of false positive (Pejaver et al., 2020). In the case of REVEL, a score above 0.5 means that the 75.4% of disease mutations are detected as pathogenic and only the 10.9% of neutral variants (Ioannidis et al., 2016). The CADD PHRED score of 31 indicates that, of all the possible substitutions of at residue 124, G124R is in the top 1% for deleterious effects. Although the MetaLR score did not directly hypothesize pathogenicity, this could be related with the lack of maximum minor allele frequency (MMAF) parameter of 1% or higher (Dong et al., 2015).

The BK channel β2 protein encoded by the *KCNMB2* gene is comprised of two transmembrane domains, TM1 and TM2, with an intervening extracellular loop and intracellular N- and C- termini facing the cytosol (Fig. 1A). Most notably, the inactivation particle (1-45aa) is located at the N-terminus, where the motif Phe-Ile-Thr (FIW) blocks the conduction pathway through the inner vestibule of the BK channel, a process that primarily occurs in the open state (Fan et al., 2020; Solaro and Lingle, 1992; Wallner et al., 1999; Wang et al., 2002; Xia et al., 1999, 2000, 2003). G124 is located in the extracellular loop (Fig. 1A) in a highly conserved region between different mammalian species (>97%) (Fig. 1B). This extracellular loop contains three asparagine residues targeted for N-glycosylation, N88, N96 and N119, relevant for the association kinetics between BK and β2 (Huang et al., 2017). Additionally, the amino acid sequence from 137 to 147 (KINQKCSYIPK) is rich in basic residues and has been proposed to be responsible for the outward rectification through an electrostatic mechanism (Chen et al., 2008; Lv et al., 2008). Finally, several cysteine residues in the extracellular loop form disulfide bonds between them as in the other β subunits (Wu et al., 2013; Zeng et al., 2003), providing a structural frame for the charybdotoxin blockage protection in which the N-glycosylations and the lysine rich sequence contribute. Thus, the location of the G124 mutation in this extracellular loop region has the potential to affect several aspects of BK/β2 channel properties.

3.3. Functional effect of the G124R mutation on non-inactivating BK current

β2 affects multiple aspects of BK channel gating, most notably conferring rapid inactivation via the hydrophobic N-terminal 'ball', but also shifting the voltage-dependence of activation to more hyperpolarized potentials and slowing the kinetics of activation (at low Ca^{2+} concentration) and deactivation (Brenner et al., 2000a; Gonzalez-Perez and Lingle, 2019). To first evaluate the inactivation properties, the initial three amino acids of the 'inactivation particle' were removed from the N-terminus (β2IR) (Wang et al., 2002; Whitt et al., 2016). HEK293T cells were transfected with BK α subunits alone, or co-transfected with $\beta2IR^{WT}$ or mutant $\beta2IR^{G124R}$ subunits. Inside-out patches were recorded in physiological Na^+ and K^+ gradients in the presence of 10 μM intracellular Ca^{2+}. These conditions mimic the K^+ driving force and intracellular Ca^{2+} concentration during neuronal

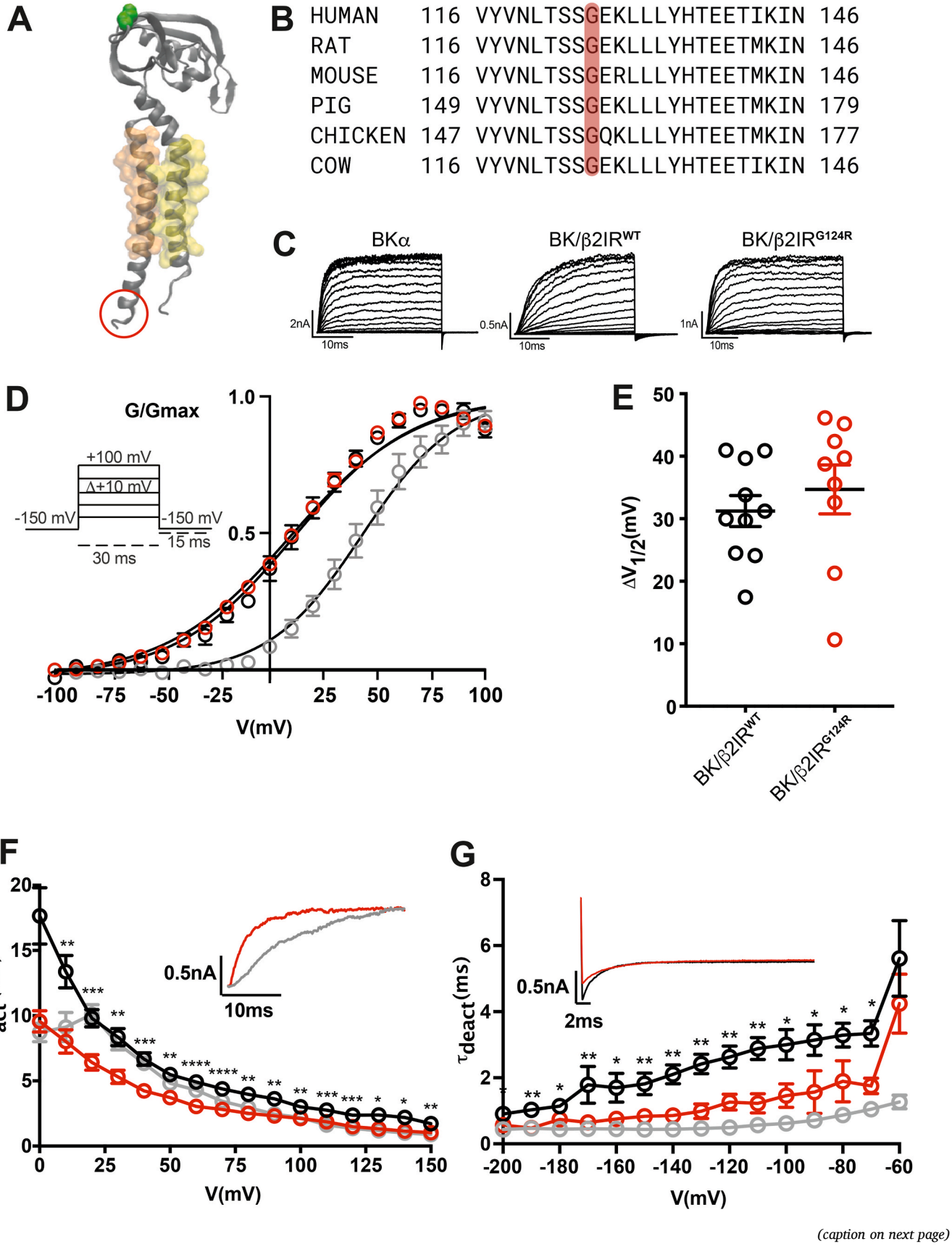

(caption on next page)

Fig. 1. The BK channel β2 subunit and assessment of the G124R mutation on BK channel properties in the absence of inactivation. (A) β2 homology model based on the β4 (PDB:6V22; Tao and MacKinnon, 2019) showing the β2 architecture with respect to transmembrane domains TM1 and TM2, localization of the G124R residue (green), and the N-terminal inactivation particle (red circle). (B) β2 amino acid sequence alignment between six different species. (C) Representative inside-out macroscopic current traces for BK/β2^{WT} and BK/β2^{G124R} in physiological K^+ and 10 μM Ca^{2+} conditions. Voltage protocol depicted in the inset in panel D. (D) Current-voltage (G–V) relationship of BK alone (gray open circles, N = 7), BK/β2IR^{WT} (black open circles, N = 10) and BK/β2IR^{G124R} (red open circles, N = 9) channels. (E) $\Delta V_{1/2}$ values (BK-only — BK/β2IR). BK/β2IR^{WT} was not different from BK/β2IR^{G124R} (P = 0.45, *t*-test). (F) Activation time constants (τ_{act}) versus voltage for BK-only (N = 7), BK/β2IR^{WT} (N = 10) and BK/β2IR^{G124R} (N = 9) channels. Inset: Representative macroscopic traces at +30 mV for BK/β2IR^{WT} (gray) and BK/β2IR^{G124R} (red) illustrating activation kinetics. The G124R mutations produces an increase in τ_{act} between 10 and + 150 mV (P < 0.02; repeated measures ANOVA with Bonferroni post-hoc). (G) Deactivation time constants (τ_{deact}) for BK-only (N = 5), BK/β2IR^{WT} (N = 10) and BK/β2IR^{G124R} (N = 9) channels. Inset: Representative traces at −80 mV for BK/β2IR^{WT} (gray) and BK/β2IR^{G124R} (red) illustrating deactivation kinetics. The BK/β2IR^{WT} channels deactivated slower compared to BK-, while the BK/β2IR^{G124R} has a less pronounced effect (P < 0.04 between −200 and −70 mV; repeated measures ANOVA with Bonferroni post-hoc). (For interpretation of the references to colour in this figure legend, the reader is referred to the Web version of this article.)

activity (Fakler and Adelman, 2008; Marrion and Tavalin, 1998). Using a square voltage step protocol, currents activated from BK/β2IR^{WT} or BK/β2IR^{G124R} were analyzed. Because expression can vary in transfected heterologous cells, only patches that elicited the maximal $V_{1/2}$ shift, indicative of the presence of 4 β2 subunits in the complexes, were analyzed.

We found the human β2 subunit shifts the voltage-dependence of activation by −26 mV compared to BK α channels alone ($V_{1/2}$: BK 36 ± 3.2 mV and BK/β2IR^{WT} 10 ± 4 mV; Fig. 1C–E). This effect was not different with mutant subunits, as BK/β2IR^{G124R} currents did not produce a significant difference in the $V_{1/2}$ compared with BK/β2IR^{WT} ($V_{1/2}$: BK/β2IR^{G124R} 7 ± 5 mV; Fig. 1D–E). Our results agree with prior studies reporting that the BK channel voltage sensitivity (Z) is not affected by β2 (Contreras et al., 2012; Orio et al., 2006). Additionally, we did not observe a significant difference in voltage sensitivity between the BK/β2IR^{G124R} channels and BK/β2IR^{WT} (Z = 0.91 ± 0.04 and 0.97 ± 0.06 respectively; Fig. 1D).

β2 subunits also affected BK channel opening and closing. Under these ionic conditions, BK/β2IR^{WT} currents did not activate differently than BK α channels alone (Fig. 1F). However, the mutation β2IR^{G124R} increased the activation kinetics (τ_{act}), with BK/β2IR^{G124R} currents activating 2 times faster than BK/β2IR^{WT} at 0 mV (Fig. 1F). At membrane potentials near the peak of an action potential (+40 mV), the τ_{act} for BK/β2IR^{G124R} currents was 4.2 ± 0.3 ms, while BK/β2IR^{WT} was 6.6 ± 0.5 ms. In contrast, with channel closing, BK/β2IR^{WT} currents deactivated up to 4 times slower than the BK channel alone (τ_{deact}; Fig. 1G). The presence of the mutation reduced this effect on closing, such that BK/β2IR^{G124R} was only 2 times slower on average (between −60 and −70 mV; Fig. 1G). At −60 mV, the τ_{deact} for BK/β2IR^{G124R} currents was 4.2 ± 0.9 ms, while BK/β2IR^{WT} was 5.6 ± 1.1 ms. Taken altogether, the net effect of the G124R mutation is restricted to channel opening (BK/β2IR^{G124R} channels activated more rapidly than BK/β2IR^{WT}) and closing kinetics (BK/β2IR^{G124R} channels deactivated more slowly than BK/β2IR^{WT}), not affecting the voltage-dependence of activation.

3.4. Effect of G124R mutation on the BK channel inactivation

Although G124R is located extracellularly, away from the N-terminal inactivation particle inside the cell, the mutation could affect inactivation by changing the kinetics for β2 modulation of BK channels. To test this, WT and G124R mutant β2 subunits with intact inactivation were used under 3 voltage protocols in physiological ionic conditions to address different aspects of this process. First, to determine how fast inactivation occurs and the basic voltage-dependence, the rate of inactivation (τ_{inact}) and the voltage at which voltage the half of the channels are inactivated ($V_{1/2\ inact}$) were obtained using a protocol stepping the BK/β2^{WT} and BK/β2^{G124R} channels from closed to different activation potentials, and then measuring the current at a post-pulse step to +160 mV (Fig. 2A and inset in 2B). BK channels co-expressed with β2^{WT} produced macroscopic currents that activated, and then inactivated, within 150 ms (Fig. 2A). As a control for α:β subunit stoichiometry, patches were first stepped to +160 mV to confirm they produced τ_{inact} values consistent with four β2 subunits per BK channel, which was 20 ms in symmetrical K^+ and 10 μM Ca^{2+} from prior studies (Wang et al., 2002). Thus, only patches with currents that produced macroscopic τ_{inact} of less than or equal to 20 ± 5 ms (±2 standard deviations from the average; Fig. 2B) were analyzed.

BK/β2^{G124R} had τ_{inact} values that were indistinguishable from BK/β2^{WT} (Fig. 2A–B). Fig. 2C shows the similar distributions from BK/β2^{WT} and BK/β2^{G124R} channels across individual patches for −20 and +60 mV, demonstrating the mutation does not cause a systematic effect. Average τ_{inact} values were 52.3 ± 5.7 ms for BK/β2^{WT} and 46.6 ± 4.5 ms for BK/β2^{G124R} at +20 mV, and 18.5 ± 1.3 ms for BK/β2^{WT} and 19.2 ± 1.3 ms for BK/β2^{G124R} at +160 mV. In addition, no difference was observed in the $V_{1/2}$ for inactivation between BK/β2^{WT} (−141 ± 5.3 mV) and BK/β2^{G124R} (−148 ± 5.7 mV) currents using the same voltage protocol (Fig. 2D–F).

Next, we assessed recovery from inactivation, previously shown to be between 18 and 25 ms in symmetrical K^+ and 10 μM Ca^{2+} conditions (Li et al., 2007; Wang et al., 2002; Xia et al., 2003). A two-pulse protocol was used, consisting of an activation step to +160 mV to allow activation and inactivation to occur, followed by a second shorter step to +160 mV after a recovery interval at −150 mV. The second step was 2 ms after the first, with increasing increments of 2 ms to evaluate the time constant of recovery from inactivation (Fig. 3A). The representative trace shows the BK/β2^{G124R} current response, with increasing amount of current obtained from each subsequent recovery step (Fig. 3A). To compare BK/β2^{WT} and BK/β2^{G124R} channel recovery from inactivation, current from second voltage step was normalized to the peak current from the first voltage step ($I_{2nd\ step}/I_{1st\ step}$; Fig. 3A) and plotted as a function of the recovery time interval (Fig. 3B). The recovery time constant ($\tau_{Recovery}$) was obtained from fits of normalized current (current after recovery normalized to initial peak current, $I_{2nd\ step}/I_{1st\ step}$) over time curves. In these experimental conditions, no difference was found between the $\tau_{Recovery}$ for BK channels co-expressed with β2^{WT} (28 ± 2.7 ms) compared to mutant β2^{G124R} (27 ± 3.3 ms) (Fig. 3C).

A final set of conditions using an action potential (AP) waveform stimulus was evaluated, a non-stationary voltage command that integrates the activation and deactivation kinetics during BK/β2 gating. The representative AP waveform was obtained from a central hypothalamic neuron type where the role for BK/β2 channel regulation of neuronal activity is well-characterized and where the alteration of BK current properties due to loss of β2 is detectable in single AP-evoked BK currents (Whitt et al., 2016). As in prior experiments, data was only included from patches with τ_{inact} value of 20 ms deviations at +160 mV ± 2 standard deviations (Fig. 4A–B) consistent with channel complexes containing 4 β2 subunits (Wang et al., 2002).

Small currents were evoked from BK/β2^{WT} co-expressed channels (Fig. 4C) using this single AP voltage stimulus in physiological K^+ conditions. BK/β2^{G124R} also reliably produced AP-evoked currents. To determine if the faster activation and slower deactivation associated with β2^{G124R} in steady-state experiments could increase AP-evoked BK current, BK current was integrated as area under the curve (AUC). AUC values were normalized to the maximum current evoked by the square voltage step protocol to account for differences in expression between patches. No differences were detected between the β2^{WT} and β2^{G124R} AP-

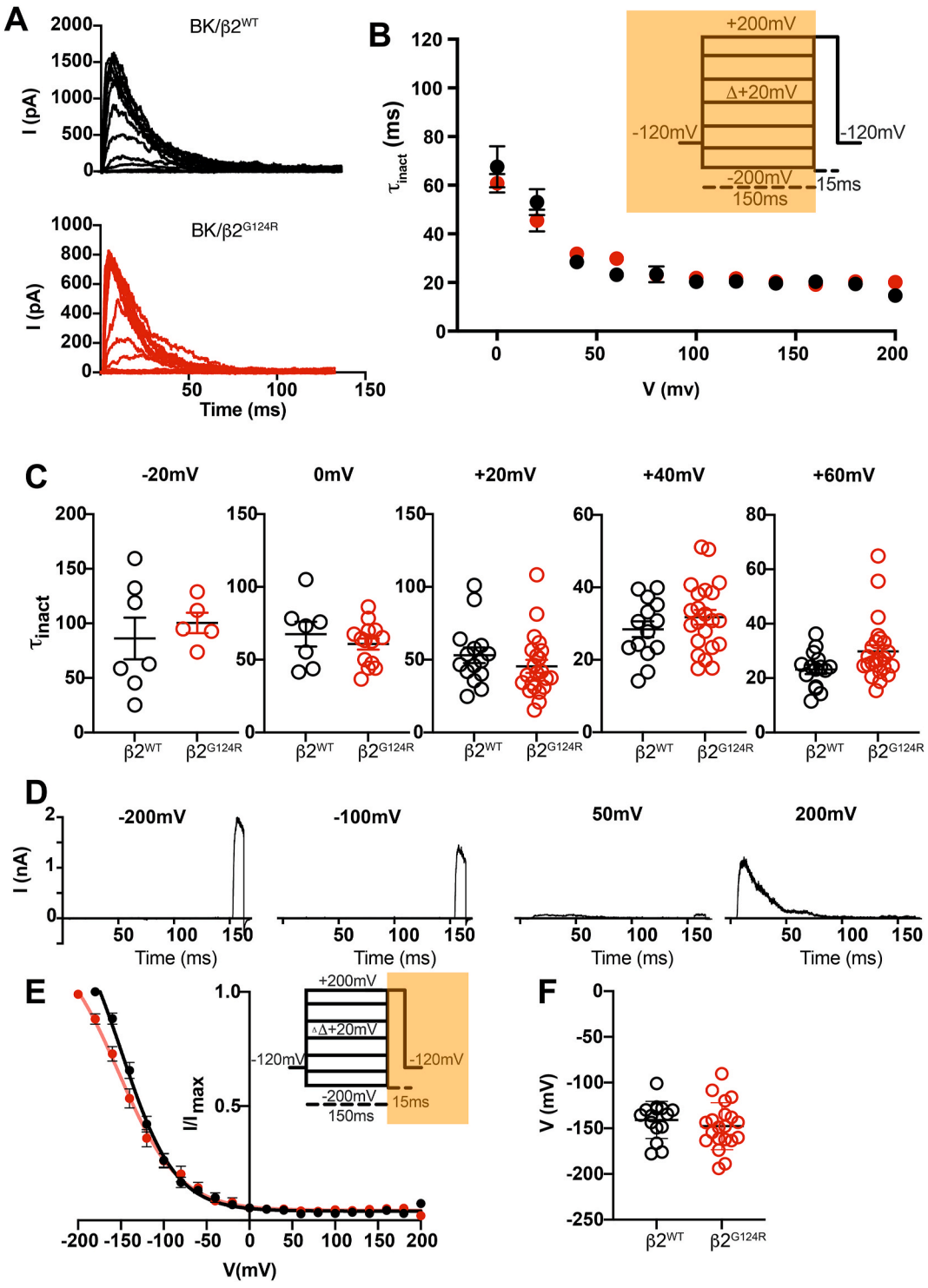

Fig. 2. Effect of the β2^{G124R} mutation on BK channel inactivation. (A) Two-step voltage protocol and representative macroscopic currents at 20 mV increments of the BK/β2^{WT} and BK/β2^{G124R}. (B) Inactivation kinetics (τ_{inact}) versus voltage, for BK/β2^{WT} (filled black circles, N = 23) and BK/β2^{G124R} (filled red circles, N = 19) co-expression. Inset applied voltage step protocol showing in orange the section used to calculate τ_{inact}. (C) Individual τ_{inact} data between −20 and + 60 mV (P≥0.05, repeated measures ANOVA). (D) Representative traces for BK current elicited from the second voltage step. (E) I/I_{max} versus voltage between BK/β2^{WT} and BK/β2^{G124R}. Inset: voltage protocol, labeled in orange the section used to obtain the $V_{1/2\ inact}$. (F) Individual $V_{1/2\ inact}$ values for BK/β2^{WT} (N = 15) and BK/β2^{G124R} (N = 20) (P = 0.05, unpaired *t*-test). (For interpretation of the references to colour in this figure legend, the reader is referred to the Web version of this article.)

evoked currents (Fig. 4D). Furthermore, no difference was found in the peak BK current elicited by either β2 subunit (BK/β2^{WT} normalized peak current: 0.03 ± 0.004; n = 16 and BK/β2^{G124R} current: 0.03 ± 0.003, n = 20; P = 0.9, *t*-test). This experiment further confirmed that the inactivation phenotype conferred by β2 is not affected by the changes in BK channel opening and closing kinetics induced by the β2^{G124R} mutation.

4. Discussion

Here we report a new *KCNMB2* mutation, c.370G > A; p.G124R,

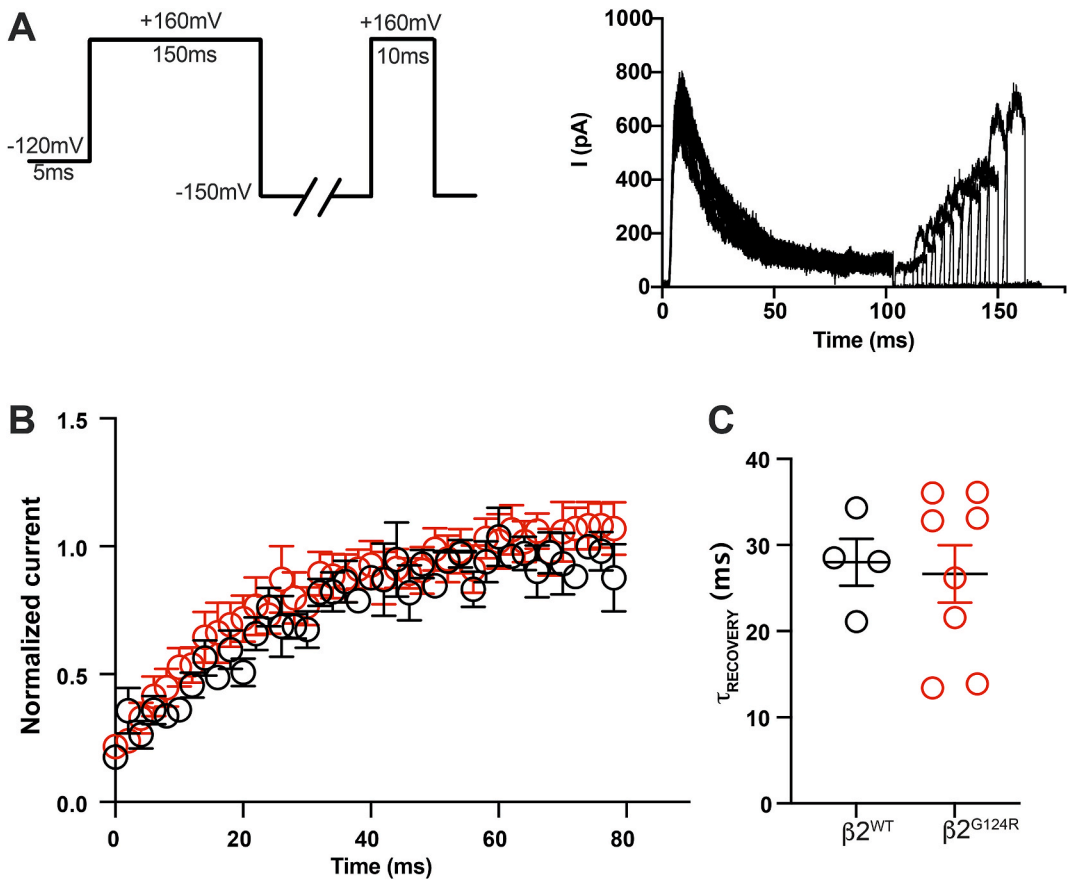

Fig. 3. Comparison BK/β2^{WT} and BK/β2^{G124R} recovery from inactivation. (A) Two-pulse voltage-step protocol and representative current trace for BK/β2^{G124R}. (B) Current from second voltage-step was normalized to the peak pre-pulse current (normalized current) and plotted as a function of the recovery time interval β2^{WT} (black, N = 4) and β2^{G124R} (red, N = 8). Normalized current curves are fitted a single exponential to calculate the recovery kinetics ($\tau_{Recovery}$). (C) Individual $\tau_{Recovery}$ values for BK/β2^{WT} and BK/β2^{G124R} (P = 0.8, unpaired *t*-test). (For interpretation of the references to colour in this figure legend, the reader is referred to the Web version of this article.)

from a heterozygous individual with autism that affects BK/β2 channel opening and closing kinetics without obvious effect on inactivation. The present investigation was not designed to establish causality for the G124R variant in ASD, due to the *de novo* nature of the mutation. As additional patient variants are reported for *KCNMB2*, it remains to be determined whether the association between this gene or variant and ASD will be substantiated in a larger ASD cohort. Nevertheless, because ASD, learning disability, and other neurodevelopmental dysfunctions are prominent phenotypes in the *KCNMA1* channelopathy patient population (Bailey et al., 2019; Miller et al., 2021; Laumonnier et al., 2006; Wu et al., 2020; Yesil et al., 2018; Song et al., 2018; Staisch et al., 2016; Sun et al., 2019), the hypothesis that *KCNMB2* could be associated with ASD is reasonable to investigate going forward (Xia et al., 2020).

In addition to reporting the patient phenotype, a basic functional investigation of the G124R mutation β2 on BK channel activity in physiological K^+ conditions revealed limited gain-of-function (GOF) effects on activation and deactivation gating kinetics (speeding activation and slowing deactivation). This kinetic effect is similar in nature, although smaller in magnitude, with two other *KCNMA1* mutations that cause seizures and dyskinesia (Moldenhauer et al., 2020; Park et al., 2022). Some of these *KCNMA1* channelopathy patients also have autism and learning disability, but ASD and intellectual/learning diagnoses are not exclusive to the GOF population and are additionally found in patients harboring loss-of-function variants (LOF) and variants of uncertain significance (VUS) (Bailey et al., 2019; Heim et al., 2020; Miller et al., 2021). Furthermore, changes in BK channel activity in both directions are associated with ASD-type phenotypes in animal and *ex vivo* human models (Deng and Klyachko, 2016; Deng et al., 2013; Perche et al., 2022; Song et al., 2018; Sun et al., 2019; Valerie Lemaire-Mayo et al., 2020). Most notably, the *KCNMA1* variant A138V, which was sequenced from an autistic patient, showed aspects of both GOF and LOF effects on BK channel activity, depending on the conditions tested (Laumonnier et al., 2006; Plante et al., 2019). Yet like β2^{G124R}, BKα^{A138V} also failed to change AP-evoked BK currents in a similar single-spike stimulation paradigm (Lai, 2015). It remains to be determined whether either of these variants directly alter neuronal activity and whether changes occur in the patient heterozygous allele configuration. Thus, at present there is not enough evidence from autism-associated *KCNMA1* variants to inform how the β2^{G124R} mutation could alter neuronal activity in a pathophysiological manner.

The effect on BK channel kinetics produced by β2 can be dissociated from inactivation. With the effects of G124R on activation and deactivation kinetics, this study provides new data implicating the TM1-TM2 loop of β2 in BK channel gating. Although few prior functional and structural studies address this role directly, G124 is upstream of 3 N-glycosylated asparagine residues: N88, N96 and N119 (Huang et al., 2017). These residues have been implicated in the association between BK and β2, charybdotoxin sensitivity, and gating kinetics (Huang et al., 2017). We did not find a notable difference in YFP intensity, or differences in the magnitude of recorded current levels, between BK/β2IR^{WT} and BK/β2IR^{G124R}-transfected HEK293T cells (tail current at +150 mV, BK/β2IR^{WT}: 294 ± 65 pA, n = 10 and BK/β2IR^{G124R}: 335 ± 50 pA, n = 9; P = 0.51, *t*-test), suggesting the mutation does not predominantly affect channel expression. However, our study did not evaluate the surface expression or charybdotoxin block of BK/β2^{G124R} compared to β2^{WT}. Functionally, despite the effects of asparagine point mutations in the β2

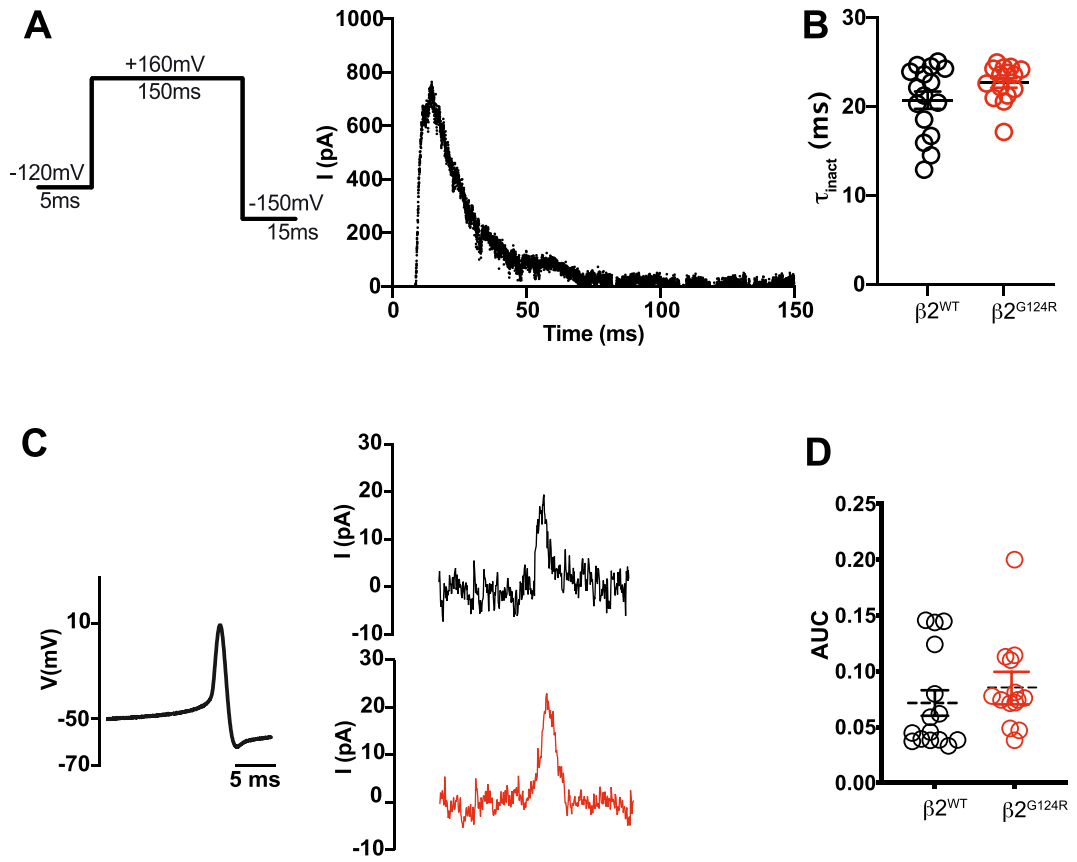

Fig. 4. BK/β2^{G124R} effects on action potential-evoked BK current under dynamic voltage conditions. (A) A pre-activation square step to +160 mV was used to verify full β2 stoichiometry (test protocol; left panel). Representative BK current from the test protocol with τ_{inact} of 16 ms. AP voltage commands were only delivered to patches where τ_{inact} was 20 ± 5 ms in the current elicited with the test protocol. (B) τ_{inact} values obtained from individual patches with the test protocol. BK co-expressed with β2^{WT} (black, N = 16) or β2^{G124R} (red, N = 20) were not different (P = 0.1, n.s unpaired *t*-test). (C) AP voltage command (left panel; $t_{1/2}$: 0.6 ms, threshold: 40 mV, and amplitude +50 mV) and representative AP-evoked currents for BK/β2^{WT} and BK/β2^{G124R} in physiological K^+, 10 μM Ca^{2+} conditions. τ_{inact} values obtained from the test protocol were 16 ms (BK/β2^{WT}) and 22 ms (BK/β2^{G124R}) for the representative examples. (D) Area under the curve (AUC, pA*ms), normalized to the maximal macroscopic current level. BK/β2^{WT} (N = 16) and BK/β2^{G124R} (N = 20) were not different (P = 0.9, unpaired *t*-test). (For interpretation of the references to colour in this figure legend, the reader is referred to the Web version of this article.)

extracellular loop on activation kinetics (Huang et al., 2017), other studies did not find differences in kinetics in the context of larger extracellular loop region chimeric swaps between β1 and β2IR (Orio et al., 2006). Interestingly, G124 lies in a stretch of residues with high homology between β1, β2, and β3, but not β4 (Gruslova et al., 2012). This raises the possibility that the similarities between β1 and β2 could have precluded the ability to detect a change in the chimeric experiments (Orio et al., 2006), leaving open the role of the extracellular loop in BK gating kinetics. Consistent with the data in this study, β2 has been shown to interact with the BKα voltage sensor, which would support a role in gating kinetics (Savalli et al., 2007).

Lastly, although the extracellular location of G124R does not predict a direct role, inactivation is the most obvious effect β2 confers on BK channel gating. An indirect effect on inactivation could be produced if BK/β2^{G124R} channels opened faster, and therefore inactivated earlier, reducing AP-evoked BK current amplitude. However, no differences in the inactivation or recovery from inactivation were found using either activation paradigm: steady-state (square step commands) or dynamic (action potential commands) voltage stimuli. The lack of difference suggests that any differences between the β2^{WT} and β2^{G124R} extracellular loop conformations that produced the kinetic effects in steady-state protocols are not enough to reveal an effect on the inactivation phenotype. This lack of effect was not due to a low number of β2 subunits present in the channel complex, since patches in this study were selected to contain the full 4 β2 subunits by τ_{inact} values (Li et al., 2007; Wang et al., 2002; Xia et al., 1999, 2003). Nevertheless, only one set of basic conditions was tested here. Additional deficits with β2^{G124R} may be uncovered with higher intracellular calcium concentrations or by using repetitive firing protocols which produce faster activation and limited recovery between action potentials.

5. Conclusions

Intellectual disability is one of the core phenotypes in *KCNMA1*-linked channelopathy. This study reports a *KCNMB2* variant found in an autistic individual and prompts continued investigation of an association between *KCNMB2* and ASD in a larger cohort. Future studies will be required to determine the biophysical mechanism by which the G124R mutation affects BK/β2 gating and whether this alters neuronal activity in ASD-related circuitry. However, the data presented here raise the possibility that *KCNMB2* variants could alter BK currents by similar kinetics means as some *KCNMA1*-linked channelopathy α subunit variants, without affecting inactivation.

Funding

This work was supported by NHLBI R01-HL102758 (A.L.M.) and the Training Program in Integrative Membrane Biology NIGMS T32-GM008181 (A.L.M.).

CRediT authorship contribution statement

Hans J. Moldenhauer: Conceptualization, research conception and data collection, statistical analysis design and execution, manuscript writing. **Ria L. Dinsdale:** data collection. **Sara Alvarez:** patient case description and sequencing. **Alberto Fernández-Jaén:** patient case description and sequencing, All authors approved the final version of the manuscript. **Andrea L. Meredith:** Conceptualization, Formal analysis, research conception and data analysis, statistical analysis design, manuscript writing, and review and critique.

Declaration of competing interest

The authors declare that they have no known competing financial interests or personal relationships that could have appeared to influence the work reported in this paper.

Acknowledgements

We thank Sotirios Keros and Crina Nimigean for comments on the manuscript.

References

Bailey, C.S., Moldenhauer, H.J., Park, S.M., Keros, S., Meredith, A.L., 2019. *KCNMA1*-linked channelopathy. J. Gen. Physiol. 151, 1173–1189. https://doi.org/10.1085/jgp.201912457.

Beecham, G.W., Hamilton, K., Naj, A.C., Martin, E.R., Huentelman, M., Myers, A.J., Corneveaux, J.J., Hardy, J., Vonsattel, J.P., Younkin, S.G., et al., 2014. Genome-wide association meta-analysis of neuropathologic features of Alzheimer's disease and related dementias. PLoS Genet. 10, e1004606 https://doi.org/10.1371/journal.pgen.1004606.

Brenner, R., Jegla, T.J., Wickenden, A., Liu, Y., Aldrich, R.W., 2000a. Cloning and functional characterization of novel large conductance calcium-activated potassium channel β subunits, hKCNMB3 and hKCNMB4. J. Biol. Chem. 275, 6453–6461.

Brenner, R., Jegla, T.J., Wickenden, A., Liu, Y., Aldrich, R.W., 2000b. Cloning and functional characterization of novel large conductance calcium-activated potassium channel β subunits, hKCNMB3 and hKCNMB4. J. Biol. Chem. 275, 6453–6461. https://doi.org/10.1074/jbc.275.9.6453.

Chen, M., Gan, G., Wu, Y., Wang, L., Wu, Y., Ding, J., 2008. Lysine-rich extracellular rings formed by hβ2 subunits confer the outward rectification of BK channels. PLoS One 3, e2114. https://doi.org/10.1371/journal.pone.0002114.

Connolly, J.J., Glessner, J.T., Hakonarson, H., 2013. A genome-wide association study of autism incorporating autism diagnostic interview-revised, autism diagnostic observation schedule, and social responsiveness scale. Child Dev. 84, 17–33. https://doi.org/10.1111/j.1467-8624.2012.01838.x.

Contractor, A., Klyachko, V.A., Portera-Cailliau, C., 2015. Altered neuronal and circuit excitability in fragile X syndrome. Neuron 87, 699–715. https://doi.org/10.1016/j.neuron.2015.06.017.

Contreras, G.F., Neely, A., Alvarez, O., Gonzalez, C., Latorre, R., 2012. Modulation of BK channel voltage gating by different auxiliary β subunits. Proc. Natl. Acad. Sci. U. S. A. 109, 18991–18996. https://doi.org/10.1073/pnas.1216953109.

Deng, P.Y., Klyachko, V.A., 2016. Genetic upregulation of BK channel activity normalizes multiple synaptic and circuit defects in a mouse model of fragile X syndrome. J. Physiol. 594, 83–97. https://doi.org/10.1113/JP271031.

Deng, P.Y., Rotman, Z., Blundon, J.A., Cho, Y., Cui, J., Cavalli, V., Zakharenko, S.S., Klyachko, V.A., 2013. FMRP regulates neurotransmitter release and synaptic information transmission by modulating action potential duration via BK channels. Neuron 77, 696–711. https://doi.org/10.1016/j.neuron.2012.12.018.

Dong, C., Wei, P., Jian, X., Gibbs, R., Boerwinkle, E., Wang, K., Liu, X., 2015. Comparison and integration of deleteriousness prediction methods for nonsynonymous SNVs in whole exome sequencing studies. Hum. Mol. Genet. 24, 2125–2137. https://doi.org/10.1093/hmg/ddu733.

El-Fishawy, P., State, M.W., 2010. The genetics of autism: key issues, recent findings, and clinical implications. Psychiatr. Clin. 33, 83–105. https://doi.org/10.1016/j.psc.2009.12.002.

Fakler, B., Adelman, J.P., 2008. Control of K_{Ca} channels by calcium nano/microdomains. Neuron 59, 873–881. https://doi.org/10.1016/j.neuron.2008.09.001.

Fan, C., Sukomon, N., Flood, E., Rheinberger, J., Allen, T.W., Nimigean, C.M., 2020. Ball-and-chain inactivation in a calcium-gated potassium channel. Nature 580, 288–293. https://doi.org/10.1038/s41586-020-2116-0.

Fitzgerald, M., 2010. Use of autism diagnostic interview (ADI-R) in clinical practice. Ir. J. Psychol. Med. 27, 160. https://doi.org/10.1017/S0790966700001403.

Gonzalez-Perez, V., Lingle, C.J., 2019. Regulation of BK channels by β and γSubunits. Annu. Rev. Physiol. 81, 113–137. https://doi.org/10.1146/annurev-physiol-022516-034038.

Gruslova, A., Semenov, I., Wang, B., 2012. An extracellular domain of the accessory β1 subunit is required for modulating BK channel voltage sensor and gate. J. Gen. Physiol. 139, 57–67. https://doi.org/10.1085/jgp.201110698.

Heim, J., Vemuri, A., Lewis, S., Guida, B., Troester, M., Keros, S., Meredith, A., Kruer, M. C., 2020. Cataplexy in patients harboring the KCNMA1 p.N999S mutation. Movement Disorder Clinic. Pract. 7, 861–862. https://doi.org/10.1002/mdc3.13024.

Huang, Z.G., Liu, H.W., Yan, Z.Z., Wang, S., Wang, L.Y., Ding, J.P., 2017. The glycosylation of the extracellular loop of β2 subunits diversifies functional phenotypes of BK Channels. Channels 11, 156–166. https://doi.org/10.1080/19336950.2016.1243631.

Hurley, M.J., Deacon, R.M.J., Chan, A.W.E., Baker, D., Selwood, D.L., Cogram, P., 2022. Reversal of behavioural phenotype by the cannabinoid-like compound VSN16R in fragile X syndrome mice. Brain 145 (1), 76–82. https://doi.org/10.1093/brain/awab246.

Ioannidis, N.M., Rothstein, J.H., Pejaver, V., Middha, S., McDonnell, S.K., Baheti, S., Musolf, A., Li, Q., Holzinger, E., Karyadi, D., et al., 2016. REVEL: an Ensemble method for predicting the pathogenicity of rare missense variants. Am. J. Hum. Genet. 99, 877–885. https://doi.org/10.1016/j.ajhg.2016.08.016.

Jaffe, D.B., Wang, B., Brenner, R., 2011. Shaping of action potentials by type I and type II large-conductance Ca^{2+}-activated K^+ channels. Neuroscience 192, 205–218. https://doi.org/10.1016/j.neuroscience.2011.06.028.

Kimbrel, N.A., Garrett, M.E., Dennis, M.F., Va Mid-Atlantic Mental Illness Research, E., Clinical Center, W., Hauser, M.A., Ashley-Koch, A.E., Beckham, J.C., 2018. A genome-wide association study of suicide attempts and suicidal ideation in U.S. military veterans. Psychiatr. Res. 269, 64–69. https://doi.org/10.1016/j.psychres.2018.07.017.

Kshatri, A., Cerrada, A., Gimeno, R., Bartolome-Martin, D., Rojas, P., Giraldez, T., 2020. Differential regulation of BK channels by fragile X mental retardation protein. J. Gen. Physiol. 152 https://doi.org/10.1085/jgp.201912502.

Lai, M., 2015. Role of BK channels in cardiac function. In: PhD Thesis. A. James Clark School of Engineering, University of Maryland College Park.

Latorre, R., Castillo, K., Carrasquel-Ursulaez, W., Sepulveda, R.V., Gonzalez-Nilo, F., Gonzalez, C., Alvarez, O., 2017. Molecular determinants of BK channel functional diversity and functioning. Physiol. Rev. 97, 39–87. https://doi.org/10.1152/physrev.00001.2016.

Laumonnier, F., Roger, S., Guerin, P., Molinari, F., M'Rad, R., Cahard, D., Belhadj, A., Halayem, M., Persico, A.M., Elia, M., et al., 2006. Association of a functional deficit of the BK_{Ca} channel, a synaptic regulator of neuronal excitability, with autism and mental retardation. Am. J. Psychiatr. 163, 1622–1629. https://doi.org/10.1176/appi.ajp.163.9.1622.

Li, H., Yao, J., Tong, X., Guo, Z., Wu, Y., Sun, L., Pan, N., Wu, H., Xu, T., Ding, J., 2007. Interaction sites between the Slo1 pore and the NH2 terminus of the β2 subunit, probed with a three-residue sensor. J. Biol. Chem. 282, 17720–17728. https://doi.org/10.1074/jbc.M607063200.

Lv, C., Chen, M., Gan, G., Wang, L., Xu, T., Ding, J., 2008. Four-turn α-helical segment prevents surface expression of the auxiliary hβ2 subunit of BK-type channel. J. Biol. Chem. 283, 2709–2715. https://doi.org/10.1074/jbc.M704440200.

Marrion, N.V., Tavalin, S.J., 1998. Selective activation of Ca^{2+}-activated K^+ channels by co-localized Ca^{2+} channels in hippocampal neurons. Nature 395, 900–905. https://doi.org/10.1038/27674.

Miller, J.P., Moldenhauer, H.J., Keros, S., and Meredith, A.L. An emerging spectrum of variants and clinical features in *KCNMA1*-linked channelopathy. Channels 15(1): 447-464. 10.1080/19336950.2021.1938852.

Moldenhauer, H.J., Matychak, K.K., Meredith, A.L., 2020. Comparative gain-of-function effects of the *KCNMA1*-N999S mutation on human BK channel properties. J. Neurophysiol. 123, 560–570. https://doi.org/10.1152/jn.00626.2019.

Nordahl, C.W., Scholz, R., Yang, X., Buonocore, M.H., Simon, T., Rogers, S., Amaral, D. G., 2012. Increased rate of amygdala growth in children aged 2 to 4 years with autism spectrum disorders: a longitudinal study. Arch. Gen. Psychiatr. 69, 53–61. https://doi.org/10.1001/archgenpsychiatry.2011.145.

Orio, P., Torres, Y., Rojas, P., Carvacho, I., Garcia, M.L., Toro, L., Valverde, M.A., Latorre, R., 2006. Structural determinants for functional coupling between the β and α subunits in the Ca^{2+}-activated K^+ (BK) channel. J. Gen. Physiol. 127, 191–204. https://doi.org/10.1085/jgp.200509370.

Park, S., Roache, C.E., Iffland, P.H., Moldenhauer, H.J., Matychak, K.K., Plante, A.E., Crino, P.B., Meredith, A.L., 2022. BK channel properties correlate with neurobehavioral severity in three *KCNMA1*-linked channelopathy mouse models. Elife 11, e77953.

Pejaver, V., Urresti, J., Lugo-Martinez, J., Pagel, K.A., Lin, G.N., Nam, H.J., Mort, M., Cooper, D.N., Sebat, J., Iakoucheva, L.M., et al., 2020. Inferring the molecular and phenotypic impact of amino acid variants with MutPred2. Nat. Commun. 11, 5918. https://doi.org/10.1038/s41467-020-19669-x.

Perche, O., Lesne, F., Patat, A., Raab, S., Twyman, R., Ring, R.H., Briault, S., 2022. Large-conductance calcium-activated potassium channel haploinsufficiency leads to sensory deficits in the visual system: a case report. J. Med. Case Rep. 16, 180. https://doi.org/10.1186/s13256-022-03387-7.

Plante, A.E., Lai, M.H., Lu, J., Meredith, A.L., 2019. Effects of single nucleotide polymorphisms in human *KCNMA1* on BK current properties. Front. Mol. Neurosci. 12, 285. https://doi.org/10.3389/fnmol.2019.00285.

Rentzsch, P., Witten, D., Cooper, G.M., Shendure, J., Kircher, M., 2019. CADD: predicting the deleteriousness of variants throughout the human genome. Nucleic Acids Res. 47, D886–D894. https://doi.org/10.1093/nar/gky1016.

Satterstrom, F.K., Kosmicki, J.A., Wang, J., Breen, M.S., De Rubeis, S., An, J.Y., Peng, M., Collins, R., Grove, J., Klei, L., et al., 2020. Large-Scale exome sequencing study implicates both developmental and functional changes in the neurobiology of autism. Cell 180, 568–584. https://doi.org/10.1016/j.cell.2019.12.036 e523.

Savalli, N., Kondratiev, A., de Quintana, S.B., Toro, L., Olcese, R., 2007. Modes of operation of the BK_{Ca} channel beta2 subunit. J. Gen. Physiol. 130, 117–131. https://doi.org/10.1085/jgp.200709803.

Schmunk, G., Gargus, J.J., 2013. Channelopathy pathogenesis in autism spectrum disorders. Front. Genet. 4, 222. https://doi.org/10.3389/fgene.2013.00222.

Schumann, C.M., Hamstra, J., Goodlin-Jones, B.L., Lotspeich, L.J., Kwon, H., Buonocore, M.H., Lammers, C.R., Reiss, A.L., Amaral, D.G., 2004. The amygdala is enlarged in children but not adolescents with autism; the hippocampus is enlarged at all ages. J. Neurosci. 24, 6392–6401. https://doi.org/10.1523/JNEUROSCI.1297-04.2004.

Shelley, C., Whitt, J.P., Montgomery, J.R., Meredith, A.L., 2013. Phosphorylation of a constitutive serine inhibits BK channel variants containing the alternate exon "SRKR". J. Gen. Physiol. 142, 585–598. https://doi.org/10.1085/jgp.201311072.

Solaro, C.R., Lingle, C.J., 1992. Trypsin-sensitive, rapid inactivation of a calcium-activated potassium channel. Science 257, 1694–1698. https://doi.org/10.1126/science.1529355.

Song, T., Liang, S., Liu, J., Zhang, T., Yin, Y., Geng, C., Gao, S., Feng, Y., Xu, H., Guo, D., et al., 2018. CRL4 antagonizes SCFFbxo7-mediated turnover of cereblon and BK channel to regulate learning and memory. PLoS Genet. 14, e1007165 https://doi.org/10.1371/journal.pgen.1007165.

Staisch, J., Du, X., Carvalho-de-Souza, J., Kubota, T., Bezanilla, F., Gomez, C., 2016. A mutation causing reduced BK channel activity leads to cognitive inpairment and progressive cerebellar ataxia. Neurology 86.

Stoodley, C.J., 2014. Distinct regions of the cerebellum show gray matter decreases in autism, ADHD, and developmental dyslexia. Front. Syst. Neurosci. 8, 92. https://doi.org/10.3389/fnsys.2014.00092.

Sun, A.X., Yuan, Q., Fukuda, M., Yu, W., Yan, H., Lim, G.G.Y., Nai, M.H., D'Agostino, G. A., Tran, H.D., Itahana, Y., et al., 2019. Potassium channel dysfunction in human neuronal models of Angelman syndrome. Science 366, 1486–1492. https://doi.org/10.1126/science.aav5386.

Tao, X., MacKinnon, R., 2019. Molecular structures of the human Slo1 K^+ channel in complex with β4. Elife 8. https://doi.org/10.7554/eLife.51409.

Tseng-Crank, J., Godinot, N., Johansen, T.E., Ahring, P.K., Strobaek, D., Mertz, R., Foster, C.D., Olesen, S.P., Reinhart, P.H., 1996. Cloning, expression, and distribution of a Ca^{2+}-activated K^+ channel β-subunit from human brain. Proc. Natl. Acad. Sci. U. S. A. 93, 9200–9205.

Valerie Lemaire-Mayo, M.P., Crusio, Wim E., , View ORCID Profile, Louette, Eric, Pietropaolo, Susanna, View ORCID Profile, 2020. Therapeutic effects of Chlorzoxazone, a BKCa channel agonist, in a mouse model of Fragile X syndrome.

Wallner, M., Meera, P., Toro, L., 1999. Molecular basis of fast inactivation in voltage and Ca^{2+}-activated K+ channels: a transmembrane β-subunit homolog. Proc. Natl. Acad. Sci. U. S. A. 96, 4137–4142. https://doi.org/10.1073/pnas.96.7.4137.

Wang, Y.W., Ding, J.P., Xia, X.M., Lingle, C.J., 2002. Consequences of the stoichiometry of Slo1 α and auxiliary β subunits on functional properties of large-conductance Ca^{2+}-activated K^+ channels. J. Neurosci. 22, 1550–1561.

Whitt, J.P., Montgomery, J.R., Meredith, A.L., 2016. BK channel inactivation gates daytime excitability in the circadian clock. Nat. Commun. 7, 10837 https://doi.org/10.1038/ncomms10837.

Wisniowiecka-Kowalnik, B., Nowakowska, B.A., 2019. Genetics and epigenetics of autism spectrum disorder-current evidence in the field. J. Appl. Genet. 60, 37–47. https://doi.org/10.1007/s13353-018-00480-w.

Wu, R.S., Liu, G., Zakharov, S.I., Chudasama, N., Motoike, H., Karlin, A., Marx, S.O., 2013. Positions of β2 and β3 subunits in the large-conductance calcium- and voltage-activated BK potassium channel. J. Gen. Physiol. 141, 105–117. https://doi.org/10.1085/jgp.201210891.

Wu, H., Li, H., Bai, T., Han, L., Ou, J., Xun, G., Zhang, Y., Wang, Y., Duan, G., Zhao, N., et al., 2020. Phenotype-to-genotype approach reveals head-circumference-associated genes in an autism spectrum disorder cohort. Clin. Genet. 97, 338–346. https://doi.org/10.1111/cge.13665.

Xia, X.M., Ding, J.P., Lingle, C.J., 1999. Molecular basis for the inactivation of Ca^{2+} and voltage-dependent BK channels in adrenal chromaffin cells and rat insulinoma tumor cells. J. Neurosci. 19, 5255–5264.

Xia, X.M., Ding, J.P., Zeng, X.H., Duan, K.L., Lingle, C.J., 2000. Rectification and rapid activation at low Ca^{2+} of Ca^{2+}-activated, voltage-dependent BK currents: consequences of rapid inactivation by a novel β subunit. J. Neurosci. 20, 4890–4903.

Xia, X.M., Ding, J.P., Lingle, C.J., 2003. Inactivation of BK channels by the NH2 terminus of the β2 auxiliary subunit: an essential role of a terminal peptide segment of three hydrophobic residues. J. Gen. Physiol. 121, 125–148. https://doi.org/10.1085/jgp.20028667.

Xia, L., Ou, J., Li, K., Guo, H., Hu, Z., Bai, T., Zhao, J., Xia, K., Zhang, F., 2020. Genome-wide association analysis of autism identified multiple loci that have been reported as strong signals for neuropsychiatric disorders. Autism Res. 13, 382–396. https://doi.org/10.1002/aur.2229.

Yesil, G., Aralasmak, A., Akyuz, E., Icagasioglu, D., Uygur Sahin, T., Bayram, Y., 2018. Expanding the phenotype of homozygous *KCNMA1* mutations; dyskinesia, epilepsy, intellectual disability, cerebellar and corticospinal tract atrophy. Balkan Med. J. 35, 336–339. https://doi.org/10.4274/balkanmedj.2017.0986.

Zeng, X.H., Xia, X.M., Lingle, C.J., 2003. Redox-sensitive extracellular gates formed by auxiliary β subunits of calcium-activated potassium channels. Nat. Struct. Biol. 10, 448–454. https://doi.org/10.1038/nsb932.